Geophys. J. Int. (2009) **179,** 687–699 doi: 10.1111/j.1365-246X.2009.04308.x

Propagation of a melting anomaly along the ultraslow Southwest Indian Ridge between 46°E and 52°20′E: interaction with the Crozet hotspot?

Daniel Sauter,[1] Mathilde Cannat,[2] Christine Meyzen,[3] Antoine Bezos,[4] Philippe Patriat,[2] Eric Humler[4] and Eric Debayle[1]

[1]*Institut de Physique du Globe de Strasbourg,* CNRS-UMR7516, *Ecole et Observatoire des Sciences de la Terre, Université de Strasbourg,* 1 *rue Blessig* 67084, *Strasbourg cedex, France. E-mail: daniel.sauter@eost.u-strasbg.fr*
[2]*Laboratoire de Géosciences Marines,* CNRS-UMR7097, *Institut de Physique du Globe,* 4 *place Jussieu* 75252, *Paris cedex* 05, *France*
[3]*Laboratoire des Sciences de la Terre,* CNRS-UMR5570, *Ecole Nationale Supérieure de Lyon, Université Claude Bernard,* 46 *Allée d'Italie* 69364, *Lyon Cedex* 07, *France*
[4]*Laboratoire de Planétologie et Géodynamique,* CNRS-UMR6112, *Université de Nantes,* 2 *rue de la Houssinière,* B.P. 92208 44322, *Nantes Cedex* 3, *France*

Accepted 2009 June 23. Received 2009 June 23; in original form 2008 September 19

SUMMARY

Regional axial depths, mantle Bouguer anomaly values, geochemical proxies for the extent of partial melting and tomographic models along the Southwest Indian Ridge (SWIR) all concur in indicating the presence of thicker crust and hotter mantle between the Indomed and Gallieni transform faults (TFs; 46°E and 52°20′E) relative to the neighbouring ridge sections. Accreted seafloor between these TFs over the past ∼10 Myr is also locally much shallower (>1000 m) and corresponds to thicker crust (>1.7 km) than previously accreted seafloor along the same ridge region. Two large outward facing topographic gradients mark the outer edges of two anomalously shallow off-axis domains on the African and Antarctic plates. Their vertical relief (>2000 m locally) and their geometry, parallel to the present-day axis along a >210-km-long ridge section, suggest an extremely sudden and large event dated between ∼8 (magnetic anomaly C4n) and ∼11 Ma (magnetic anomaly C5n). Asymmetric spreading and small ridge jumps occur at the onset of the formation of the anomalously shallow off-axis domains, leading to a re-organization of the ridge segmentation. We interpret these anomalously shallow off-axis domains as the relicts of a volcanic plateau due to a sudden increase of the magma supply. This event of enhanced magmatism started in the central part of the ridge section and then propagated along axis to the east and probably also to the west. However, it did not cross the Gallieni and Indomed TFs suggesting that large offsets can curtail or even block along-axis melt flow. We propose that this melting anomaly may be ascribed to a regionally higher mantle temperature provided by mantle outpouring from the Crozet hotspot towards the SWIR.

Key words: Magnetic anomalies: modelling and interpretation; Mid-ocean ridge processes; Hotspots; Indian Ocean.

1 INTRODUCTION

Hotspot–ridge interactions induce physical and chemical anomalies along a significant portion (15–20 per cent) of the global mid-ocean ridge system (Ito *et al.* 2003). Near or on ridge plumes decrease the depth of the ridge axis, thicken the oceanic crust and leave an imprint on the mid-ocean ridge geochemistry. By far, the largest and best studied example of ridge–hotspot interaction is Iceland, where the mid-Atlantic Ridge (MAR) axis rises above sea level and is underlain by a region of low mantle velocities being interpreted as a hot plume (e.g. White *et al.* 1995; Wolfe *et al.* 1997; Searle *et al.* 1998; Pilidou *et al.* 2005). The amplitude of bathymetry and gravity anomalies is maximum on such on-axis hotspots and decreases with increasing ridge–hotspot distance (Ito & Lin 1995; Ribe *et al.* 1995). The along-axis length of these bathymetry and gravity anomalies, however, depend inversely on spreading rate, reflecting the extent to which plume material will flow along axis before being swept away by the spreading lithosphere (Ito & Lin 1995; Ribe *et al.* 1995).

The importance of thick lithosphere resulting from plate cooling with age and from large transform offsets in controlling the style of ridge–hotspot interaction in ultraslow spreading environments has been pointed out by Georgen *et al.* (2001) and Georgen & Lin

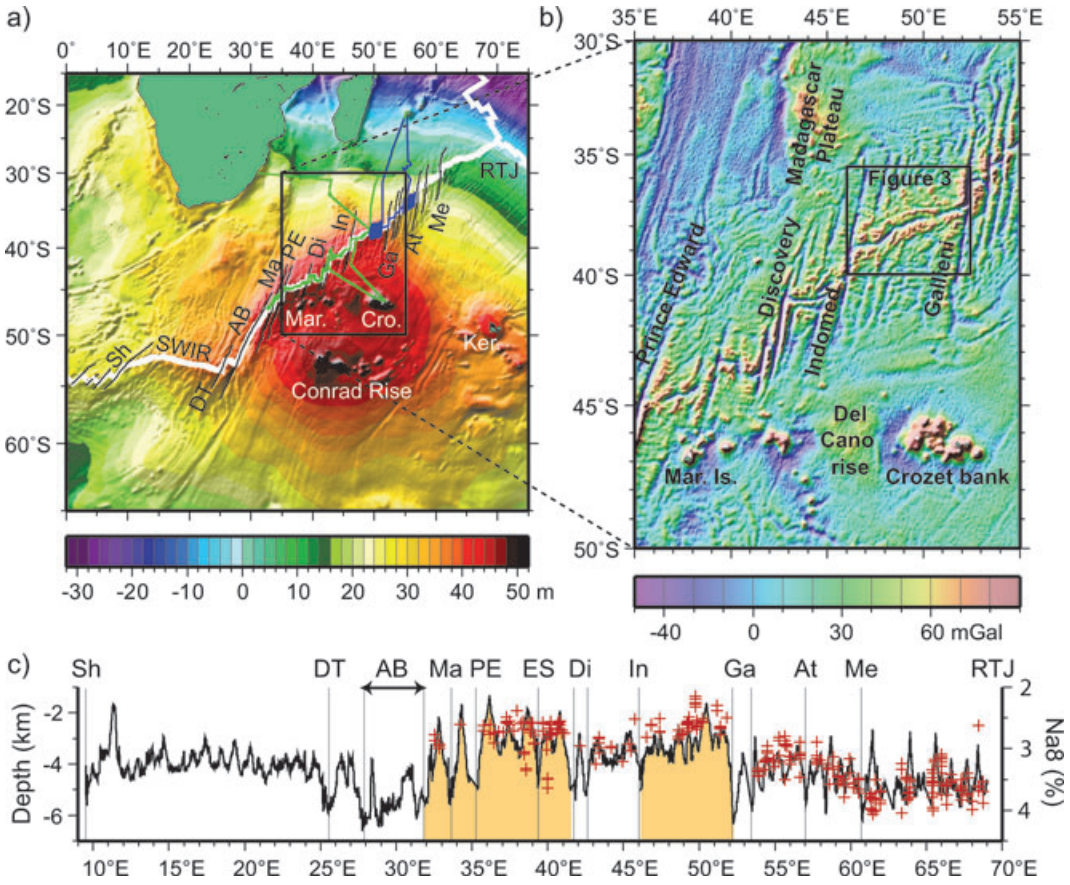

Figure 1. Geoid topography in the southwestern Indian ocean (a), free air gravity anomalies over the central part of the Southwest Indian Ridge (SWIR) (b) and along-axis bathymetric profile compared to the along-axis variation of the $Na_{8.0}$ composition of basalts glasses dredged along the SWIR axis (c). Black and white lines in the geoid topography map indicate the fractures zones and the SWIR axis, respectively. The green and blue lines show tracks of the SWIFT and GALLiENi cruises, respectively. Sh: Shaka TF; DT: Du Toit TF; AB: Andrew Bain TF; Ma: Marion TF; PE: Prince Edward TF; ES: Eric Simpson TF; Di: Discovery I and II TFs; In: Indomed TF; Ga: Gallieni and Gazelle TFs; Me: Melville TF; RTJ: Rodrigues Triple Junction; Mar.: Marion Island; Cro.: Crozet Archipelago; Ker.: Kerguelen Island. Free air gravity anomalies are derived from satellite sea-surface altimeter measurements (Sandwell & Smith 1997). The along-axis bathymetric profile was drawn using the multibeam bathymetric data collected during the SWIFT cruise on board of the R/V Marion Dufresne in 2001 (in green on the geoid map) merged with existing multibeam bathymetric data from the RODRIGUES cruises (Munschy & Schlich 1990), the CAPSING cruise (Patriat *et al.* 1997), the GALLiENi cruise (in blue on the geoid map; Sauter *et al.* 2001), the KN145L16 cruise (Grindlay *et al.* 1998) and the KN162 cruise (Dick *et al.* 2003). The along-axis variation of the $Na_{8.0}$ composition (red crosses) of basaltic glasses is from Cannat *et al.* (2008) [the subscript 8.0 refers to values corrected for low-pressure fractionation to a common MgO content of 8 wt per cent, as described by Klein & Langmuir (1987)]. The orange areas indicate the two ridge sections with prominent shallow bathymetry.

(2003). The Southwest Indian Ridge (SWIR) is among the world's slowest-spreading ridges with a full spreading rate of ∼14 km Myr^{-1} (at 64°E/28°S, Patriat *et al.* 1997; Chu & Gordon 1999). Together with the ultraslow-spreading Arctic ridges, the SWIR makes up a significant proportion of the global oceanic ridge system (about 20 per cent of the total length of ridges spreads at rates less than 20 km Myr^{-1}; Bird 2003). Both the Bouvet and Marion hotspots have significant effects on the accretionary processes in the western and central portion of the SWIR, respectively (Georgen *et al.* 2001). By contrast, the Crozet hotspot, located at ∼1000 km south of the ridge axis (Fig. 1) is thought to have presently no interaction with the ridge (Meyzen *et al.* 2005).

Using available off-axis bathymetry, gravity and magnetic data, we show evidence for a transient event of enhanced magmatism occurring along the central part of the SWIR between the Indomed transform fault (TF) and the Gallieni TF (46°E and 52°20′E, respectively). We interpret this event as due to more pronounced interactions between the SWIR and the Crozet hotspot in the recent past (<10 Ma).

2 GEOLOGICAL SETTING

The SWIR (Fig. 1) is among the world's slowest-spreading ridges. Between the Prince Edward TF (35°30'E) and the Rodrigues Triple Junction (70°E) the SWIR separates Somalia and Antarctica with an almost constant spreading rate of ∼14 km Myr^{-1} (Horner-Johnson *et al.* 2005). The compilation of multibeam bathymetric data along the axial valley of the SWIR reveals two shallow regions of the ridge (Fig. 1c). The western one, near the Marion Island, has a 3090 m mean axial depth and is bounded by the Prince Edward TF and the Discovery TF, which offset the ridge by about 720 and 350 km, respectively. The eastern shallow region is located at ∼1000 km to the north of the Crozet hotspot and is bounded by the Indomed and Gallieni TFs which offset the ridge axis by about 145 and 115 km, respectively (corresponding to ∼20 and ∼16 Myr age offsets, respectively). The mean axial depth reaches 3180 m between these two TFs. The axis runs deeper (3530 m) between the Discovery and Indomed TFs. To the east of the Gallieni TF, axial depths increase, reaching a mean value of 4730 m in the deepest

part of the ridge, between the Melville TF (61°E) and the Rodrigues Triple Junction. These large-scale (>200 km) variations in axial depths of the SWIR appear primarily owing to heterogeneities in mantle temperature (Cannat *et al.* 1999b, 2008). Despite some local compositional complexities, regional averages of sodium content of SWIR basalts ($Na_{8.0}$ corrected for the effect of low-pressure fractional crystallization to a common MgO content of 8 wt. per cent) are well correlated with the regional axial depths along the ridge (Cannat *et al.* 2008). These regional averages of the $Na_{8.0}$ contents of basalts are commonly used to evaluate melt supply variations along the mid-ocean ridge system (Klein & Langmuir 1987). Between the Andrew Bain TF system and the Gallieni TF, the along-axis variations of $Na_{8.0}$ content of basalts mimic the axial depth variations (Fig. 1c). Two subsections with a lower mean $Na_{8.0}$ (indicating higher partial melting degree) are separated by a small subsection between the Discovery and Indomed TFs, where $Na_{8.0}$ is on average slightly higher (indicating lower partial melting degree). Both axial depths and basalt $Na_{8.0}$ content steadily increase to the east of Gallieni TF (Fig. 1c), suggesting a progressive eastward decrease of the ridge's melt supply. This increase in $Na_{8.0}$ contents of basalts is correlated with a decrease in their $Fe_{8.0}$ contents (Meyzen *et al.* 2003). This is consistent with an eastward decrease in the mean pressure of mantle melting (Klein & Langmuir 1987), and suggests lower mantle temperature in the east (Meyzen *et al.* 2003). Very low-degrees of melting of abyssal peridotites were also inferred from the Cr/(Cr+Al) ratio in spinels along the 61–64°E section of the SWIR (Seyler *et al.* 2003).

The Marion hotspot has been purported to have formed the Karoo flood basalts in Southern Africa 184 Ma ago (e.g. Morgan 1981) and may thus be one of the oldest active hotspots. It is also proposed as a source of the Cretaceous flood basalts in Madagascar (Mahoney *et al.* 1991; Storey *et al.* 1995). Subsequent to the Madagascar volcanism, the plume would have created the Madagascar Plateau (Fig. 1b), which is considered as being the Late Cretaceous-Tertiary trace of the Marion hotspot on the African Plate (Storey *et al.* 1995). Marion Island (37°51'E 46°52'S) which is located on 28 Ma crust about 250 km from the SWIR axis (Fig. 1b) marks the current location of the Marion plume (Duncan 1981). A thicker crust and/or a hotter mantle near Marion Island are revealed by a prominent mantle Bouguer anomaly (MBA) low (Georgen *et al.* 2001). Along the SWIR, axial flow driven by the Marion plume is likely curtailed by the long-offset Andrew Bain and Discovery II TFs (Georgen & Lin 2003). Marion hotspot lacks Indian Ocean isotope attributes (e.g. DUPAL) and has more mid-Ocean ridge basalts (MORB) rather than Ocean-Island basalts (OIB) like isotope attributes (Mahoney *et al.* 1992; Meyzen *et al.* 2005).

Montelli *et al.* (2004) proposed a common source for the Kerguelen and Crozet plumes, at a point located north of Crozet archipelago, in the deep lower mantle (down to 2350 km). The Crozet hotspot trace, however, is not well determined and the past and present history of this plume is controversial (Curray & Munasinghe 1991; Müller *et al.* 1993; O'Neill *et al.* 2003). The Crozet Plateau is composed of two distinct highs: the Del Cano Rise to the west and the Crozet Bank to the east (Fig. 1b). The Crozet Bank (48–53°E, 46°S) capped by volcanic islands is on average shallower than the Del Cano Rise and is interpreted as the present-day surface expression of the plume (Recq *et al.* 1998). Recent volcanism has occurred on the Crozet Islands at least for the last 9 Ma (Chevallier & Nougier 1981) and produced OIB type lavas (Giret *et al.* 2002). Crustal seismic velocities below the Crozet Bank are similar to those observed below the Kerguelen-Heard Plateau (Charvis *et al.* 1995; Recq *et al.* 1998). However, seismic refraction data show that the uppermost section of the igneous crust, probably made up of highly altered basalts, is much thicker (2–4 km) below the Crozet Bank than below the Kerguelen Plateau (Recq *et al.* 1998). The seismic crustal thickness of 10–16.5 km beneath the Crozet Bank is similar to the mean thickness determined for plume-affected structures (Recq *et al.* 1998). Unlike below the Hawaiian Islands and the Marquesas Islands, no underplated material underlies the crust of the Crozet Bank (Recq *et al.* 1998). Crustal seismic velocities correspond to densities, which preclude an airy-type isostatic response of the lithosphere to the load of the Crozet Bank (Recq *et al.* 1998). Gravity modelling further suggests that the Del Cano Rise formed near or on the SWIR axis before Early Eocene (magnetic anomaly C24n; Goslin & Patriat 1984) and is locally supported by a thickened crust whereas the Crozet Bank was emplaced off-axis, on older (Lower Cretaceous; magnetic anomaly C32n; Goslin & Patriat 1984) and cooler oceanic lithosphere and may be maintained at relatively shallow depths by an active thermal anomaly (Courtney & Recq 1986; Goslin & Diament 1987). A prominent geoid high (Fig. 1a) supports an upper-mantle thermal origin for the uplift of the Crozet Bank (Courtney & Recq 1986). The geoid/topography ratio over the bank is similar to that observed on other oceanic hotspot swells (Monnereau & Cazenave 1990). In contrast, the geochemical evidences for a contribution of the Crozet plume along the SWIR are unclear. Its isotopic composition has not yet been as well investigated as that of other Indian hotspots, and is represented by a very sparse sampling (Hedge *et al.* 1973; Dupré & Allègre 1983; Mahoney *et al.* 1996; Salters & White 1998). Less than 10 samples have been entirely characterized in Sr-Nd-Pb isotopes (Mahoney *et al.* 1996). In this framework, the isotopic signatures ($^{87}Sr/^{86}Sr$, $^{206}Pb/^{204}Pb$, $^{207}Pb/^{204}Pb$ or $^{208}Pb/^{204}Pb$ and $^{143}Nd/^{144}Nd$) of basalts dredged along the ridge axis north of the Crozet Bank show no obvious affinities with those of the Crozet hotspot (Mahoney *et al.* 1992; Meyzen *et al.* 2005). However, the SWIR signatures cannot be explained without the presence of an oceanic island type component in the mantle source (Meyzen *et al.* 2005, 2007), similar to the 'C' component of Hanan & Graham (1997). In addition, low $^{4}He/^{3}He$ ratios are also observed in basalts collected between 48°40'E and 51°10'E which further argues in favour of the presence of a primitive component in the mantle source (Meyzen 2002; Gautheron *et al.* 2008, submitted). This hotspot like component required to explain the SWIR MORB mixing relationships, may have been entrained into the SWIR MORB mantle flow field by mantle thermal plumes (Meyzen *et al.* 2005, 2007). Nonetheless, the very few available helium isotopic data for Marion, Prince Edward and Crozet Islands show more MORB-like rather than ocean-island like isotope signatures (Kurz 1982; Doucelande 2000).

3 DATA ANALYSIS

Detailed mapping of the axial valley is now available almost over the entire length of the SWIR. The most recently acquired multibeam data covers the axis between 32°E and 49°E (Figs 1 and 2) and was acquired during the SWIFT cruise on board of the R/V Marion Dufresne in 2001. We used these bathymetric data merged with existing multibeam data of the GALLiENi cruise (Sauter *et al.* 2001; Mendel *et al.* 2003; Figs 2 and 3) to refine the MBA map of Georgen *et al.* (2001) which was calculated using the GEBCO-97 bathymetric map (5′ grid spacing) of Fisher & Goodwillie (1997) and satellite-derived free air anomaly data (2′ grid spacing global gravity database of Sandwell & Smith 1997). Because no gravity data was collected during the SWIFT cruise, we merged, between

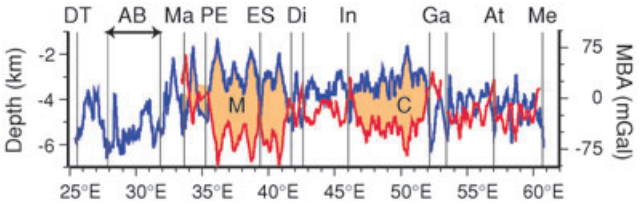

Figure 2. Bathymetric profile (in blue) and variation of the mantle Bouguer anomaly (MBA in red) along the axis of the SWIR between the Du Toit and the Melville TFs. The two ridge sections with prominent MBA lows and shallow bathymetry are shown in orange. M and C indicate the longitude of the Marion and Crozet Islands, respectively. The MBA to the east of the Gallieni TF is from Rommevaux-Jestin *et al.* (1997). DT, AB, Ma, PE, ES, Di, In, Ga and Me as in Fig. 1.

the Andrew Bain and Gallieni TFs, free air anomaly data from the GALLiENi cruise (Sauter *et al.* 2001) and satellite-derived free air anomaly data. The effect of a constant thickness (5 km), constant density (2700 kg m^{-3}) crust was removed from these free air anomaly data to obtain MBA values (Figs 2 and 3c). This new MBA map, which was calculated with multibeam bathymetric data is more reliable and has a higher resolution than the MBA map of Georgen *et al.* (2001). It shows similar long-wavelength trends but differs at the shorter-wavelength scale of ridge segments. For areas with significant bathymetric coverage (i.e. the region mapped during the GALLiENi cruise between 49° and 51°E), we also used the gravity-derived crustal thickness map published by Mendel *et al.* (2003) (see Fig. 3d).

We also used magnetic anomalies in order to refine the spreading history of the SWIR between the Indomed and Gallieni TFs. We used off-axis magnetic data collected during the GALLiENi (Sauter *et al.* 2004) and SWIFT cruises (Fig. 3). Total magnetic field data were collected during both cruises using towed proton precession magnetometers along approximately north–south flow line parallel profiles. We also re-analysed three isolated magnetic profiles (md121, gal02 and rco14), which cross the ridge to the east of 49°E (Fig. 3). Mean spreading rates and magnitudes of spreading asymmetry between magnetic anomalies C1n.o-C3An.y and C3An.y-C5n.o are given in Mendel *et al.* (2003) for the GALLiENi survey area (y and o stand for the young and old edge of the magnetic block, respectively). Here, we analyse selected magnetic anomaly profiles (Fig. 3) by performing simple 2-D forward modelling to identify magnetic anomalies C2An.y (2.581 Ma), C3n.y (4.18 Ma), C3An.y (5.894 Ma), C4n.o (8.072 Ma) and C5n.o [10.949 Ma; ages are from the geomagnetic reversal timescale of Cande & Kent (1995)].

4 RESULTS

4.1 Along-axis bathymetric and gravimetric variations between the Andrew Bain and Gallieni TFs

Gravity anomalies reflect the density structure of the crust and upper mantle. MBA lows correspond to thicker constant density model crust, or to lighter material whereas MBA highs correspond to thinner constant density model crust or to denser crustal or upper-mantle material. MBA shows pronounced intermediate- to long-wavelength trends along the SWIR (Fig. 2). From west to east, MBA values decrease from a high at the Andrew Bain TF (Georgen *et al.* 2001) to a regional low (up to −99 mGal) between the Prince Edward and Discovery TFs (Fig. 2). This prominent MBA low is interpreted as due to thicker crust and/or a hotter mantle near Marion Island (Georgen *et al.* 2001). Further east MBA values decrease again from a regional high between the Discovery and Indomed TFs to a regional low (−84 mGal) bounded by the Indomed and Gallieni TFs. This second local MBA low corresponds to our study area (Fig. 3). To the east of the Gallieni TF, MBA values increase again and the ridge deepens towards the Melville TF (Cannat *et al.* 1999b). The ridge axis is highly oblique there (56° mean ridge azimuth) whereas it is less oblique between the Discovery and Gallieni TFs (∼70° mean ridge azimuth; Cannat *et al.* 2008).

The bathymetric and gravimetric signature of the small-scale segmentation also varies along the SWIR axis. Long (>70 km) and high-relief segments (up to 2400 m) corresponding to marked MBA lows characterize the relatively shallow ridge section between the Prince Edward and Discovery TFs (Fig. 2). It is likely that this segmentation reflects robust magmatism due to the Marion hotspot (Georgen *et al.* 2001). By contrast, the section between the Discovery and Gallieni TFs reveals much shorter segments (<40 km) with lower relief (<1400 m) except in the shallowest part of the ridge section at 50°30'E (Fig. 2). In this ridge section, a long (85 km) and high relief segment (>1900 m) with a pronounced MBA low (Fig. 3c) has been interpreted as a magmatically robust segment by Sauter *et al.* (2001). The axial valley disappears at the centre of this segment [segment #27 following the nomenclature of Cannat *et al.* (1999b)] where numerous flat-topped volcanoes are observed (Mendel *et al.* 2003). The first active hydrothermal vent field discovered in 2007 along the SWIR is located at the western end of this segment #27 (Tao *et al.* 2007).

4.2 Off-axis bathymetric and gravimetric variations between the Indomed and Gallieni TFs

Off-axis bathymetric data between the Indomed and Gallieni TFs (Fig. 3a) show the presence of anomalously shallow seafloor extending on both ridge flanks. The deepening of the seafloor with age does not follow a simple subsidence curve. Instead two outward facing topographic gradients with >2000 m of vertical relief locally bound two off-axis domains of anomalously elevated seafloor (hereafter called shallow off-axis domains; Figs 3 and 4). This step-like deepening of the seafloor is clearly distinct from the progressive deepening of seafloor with age estimated using the empirical depth (D) versus age (t) curve of Parsons & Sclater (1977) $D(t) = 340t^{1/2} + D(t = 0)$ and assuming symmetrical spreading about the location of the present-day axis (Fig. 4). Shipboard bathymetry, gravity and magnetic data over the two large outward facing slopes marking the outer edges of the shallow off-axis domains are available only in the 49°20′E to 51°20′E region (Fig. 3). In this region, these outward facing slopes are located at 30–70 km from the axis on both plates. Their average slope is ∼10° with rare and steeper faults scarps (Fig. 4). Detailed multibeam bathymetric maps of these outward facing slopes as well as those of most of the shallow off-axis domains reveal rounded shaped features suggesting a volcanic constructional origin (Mendel *et al.* 2003; Fig. 5). Towards the axis the shallow off-axis domains on both plates are bounded by the walls of the present-day axial valley. The shallower seafloor at the centre of segment #27, where the axial valley disappears, connects the southern and northern shallow off-axis domains (Figs 3 and 4). The seafloor there is almost flat (see profile G25 in Figs 3 and 4). The axial valley is present at the eastern and western ends of segment #27, and narrows towards the segment centre (Fig. 3a). Such shallow off-axis domains are not observed neither to the east of the

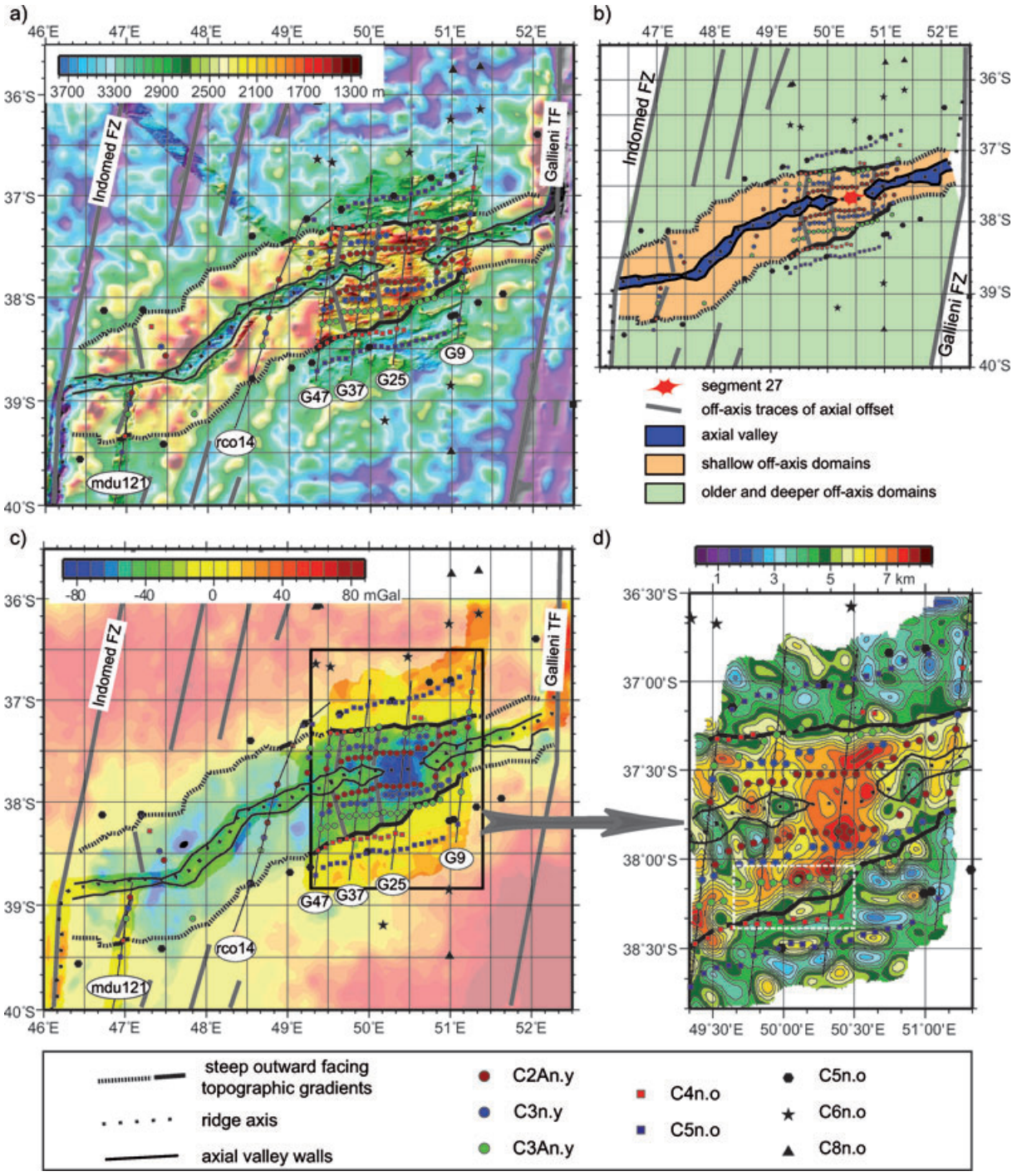

Figure 3. Magnetic anomaly identifications superimposed to the (a) bathymetric map, (b) physiographic sketch, (c) MBA map of the SWIR between the Indomed and the Gallieni TFs and (d) the gravity-derived crustal thickness map of Mendel *et al.* (2003) between 49°15'E and 51°20′E. Multibeam bathymetric data (in bright colours) from the SWIFT and the GALLiENi cruises were merged with a 2' grid of predicted seafloor depths from satellite data (in light colours) (Smith & Sandwell 1997). Black hexagons are C5n.o (10.949 Ma) identifications from Lemaux *et al.* (2002). Black stars and triangles are C6n.o (20.131 Ma) and C8n.o (26.554 Ma) identifications from Patriat *et al.* (2008). The MBA calculated with multibeam bathymetric data is shown in bright colours whereas light colours correspond to the MBA calculated with the GEBCO bathymetric map (Fisher & Goodwillie 1997). The thin black lines indicate the location of the profiles shown in Figs 4 and 6: G9, G25, G37, G47 of the GALLiENi cruise (Sauter *et al.* 2001), mdu121 of the SWIFT cruise and rco14 of the RC1401 cruise. Colour and contour intervals are every 400 m in the crustal thickness map. The white dashed frame in the crustal thickness map shows the location of Fig. 5.

Gallieni TF (Mendel *et al.* 2003) nor to the west of the Indomed TF (Figs 1 and 4).

The width of the shallow off-axis domains on each plate, as defined by the axial valley walls and by the outward-facing outer slopes, is almost constant (50–60 km) in the >210-km-long ridge region between ∼47°15'E and ∼49°30'E (Fig. 3). Isolated magnetic profiles available in this region (Figs 3 and 6) show that the outward-facing outer slopes correspond to crustal ages between

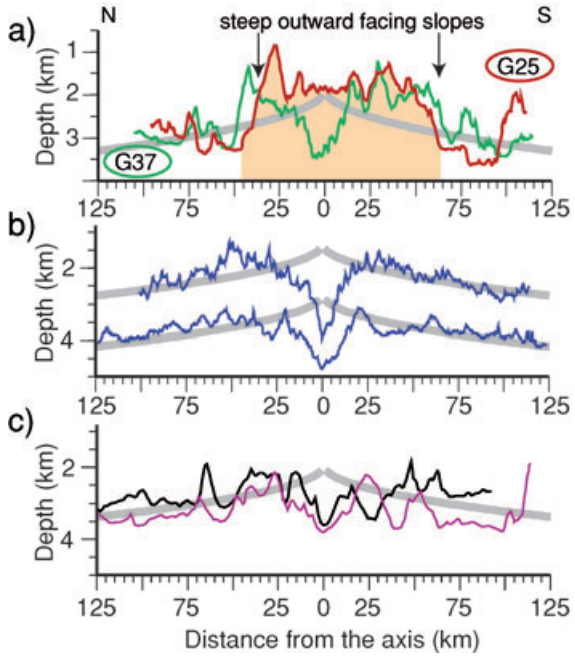

Figure 4. Comparison between across-axis depth profiles in (a) the Indomed–Gallieni TFs region (profiles G25 in red and G37 in green), (b) the Gallieni–Atlantis II TFs region and (c) the Indomed–Discovery TFs region with the deepening of the lithosphere with age (grey profiles) estimated using the empirical depth (D) versus age (t) curve of Parsons & Sclater (1977) $D(t) = 340t^{1/2} + D(t = 0)$ and assuming symmetrical spreading about the location of the present-day axis. The deepening of the seafloor with age between the Indomed and Gallieni TFs does not follow a simple subsidence curve but, two outward facing topographic gradients with >2000 m of vertical relief locally bound two off-axis domains of anomalously elevated seafloor. Such shallow off-axis domains are not observed neither to the east of the Gallieni TF nor to the west of the Indomed TF. Multibeam bathymetric profiles between the Gallieni and Atlantis II TFs cross the axis at 55.2°E in the shallowest part of a segment and at 55.6°E in a deep non-transform discontinuity, respectively (after Mendel *et al.* 2003). They follow more or less the subsidence curves. Single beam bathymetric profiles between the Indomed and Discovery TFs are from cruise MD34 of the R/V Marion Dufresne and cross the axis at 43.7°E and 44.8°E, respectively (Patriat *et al.* 2008). They show a rough topography, which oscillates around the subsidence curve. All profiles strike ∼NS.

∼8 Ma (magnetic anomaly C4n.o) and ∼11 Ma (C5n.o), and confirm that the full spreading rate is almost constant for the last ∼11 Myr (14–15 km Myr^{-1}; Mendel *et al.* 2003). To the west of 47°15'E, the width of the shallow off-axis domains appears to decrease towards the Indomed TF but the lack of shipboard bathymetry and of suitably oriented magnetic profiles does not allow further analysis. To the east of 49°30'E, the width of the shallow off-axis domains also decreases towards the Gallieni TF (Fig. 3). Shipboard bathymetry and tight magnetic profiles available in the GALLiENi survey area allow us to detail this evolution between 49°30'E and 51°20′E (Fig. 3). In this ∼160-km-long ridge region, the outer slopes of the shallow off-axis domains draw a V pointing eastward and are clearly oblique to the magnetic isochrones (Fig. 3). Based on magnetic isochrones, the age of the southern branch of this V to the east of 49°30'E is estimated to decrease from ∼8.1 Ma (C4n.o) at 49°50'E, ∼6.6 Ma (C3An.o) at 50°20′E, to ∼5.9 Ma (C3An.y) at 50°40'E, ∼5.2 Ma (C3n.o) at 51°E and to ∼4.2 Ma (C3n.y) at 51°10'E (Fig. 6). The age of the northern branch of the V is more difficult to determine because magnetic anomalies C4n and C3An are poorly defined in the northern plate (Fig. 6). Forward modelling suggests that this could be due to strongly asymmetric spreading (30–70 per cent) during the corresponding time interval, resulting in the coalescence of these two anomalies (see profile G37 in Fig. 6). This asymmetric spreading, with a higher rate in the southern plate, would have been occurring at the onset of the formation of the shallow off-axis domains. Asymmetric spreading would also explain why the off-axis shallow domain in the GALLiENi survey area, is significantly wider in the southern plate than in the northern plate (∼60 km against ∼40 km at 50°E, see profiles G25 and G37 in Fig. 6).

Bathymetry and the crustal thickness variation map modelled from gravity data in the GALLiENi survey area (Fig. 3d; Mendel *et al.* 2003) reveal that the seafloor is on average 1000 m shallower, and the crust 1.7 km thicker beneath the shallow off-axis domains (average seafloor depth 2080 ± 350 m; average crustal thickness 6.1 ± 0.8 km), than beneath the older and deeper off-axis domains (average seafloor depth 3050 ± 310 m; average crustal thickness 4.4 ± 0.8 km). This is illustrated in Fig. 7, where seafloor depth and modelled crustal thickness are plotted along Chrons C2An.y and C5n.o in the African and Antarctic plates. On top of the shallow off-axis domains, the seafloor is about 1 km shallower along Chron C2An.y than along Chron C5n.o (Fig. 7). The differences between the mean crustal thickness calculated along these two Chrons fall in the range 1.4–2.4 km. The maximum model crustal thickness corresponds to the present-day ridge axis at the centre of segment #27. The model crust there is 3 km thicker than in the older and deeper seafloor outside the shallow domain (see profile G25 in Fig. 6). On average, the model crust on-axis in the Gallieni survey area is 0.8 km thinner than over the shallow off-axis domains. However, the gravity-derived crustal thickness model neglects lateral density variations. While this assumption may be valid, at least as a working hypothesis, in the off-axis areas, it is unlikely to be so on axis, where local melt concentrations would modify the density structure, and where the thermal structure is most poorly constrained. For this reason, the gravity-derived crustal thickness variations between the axial area and the off-axis domains should be taken with caution.

The off-axis bathymetry predicted from satellite data shows no stable off-axis trace of the segmentation in the old and deep off-axis domains between 49°E and the Gallieni TF (Fig. 3a). The bathymetric highs there are randomly distributed (Mendel *et al.* 2003). There is no continuity between the axial segmentation and the gravity structure in these old and deep off-axis domains, indicating that the present-day segmentation was not established prior the formation of the shallow off-axis domains. The obliquity of the present-day axis between 49°E and the Gallieni TF is lower than between 49°E and the Indomed TF where a large axial non-transform discontinuity offset the ridge by >70 km. This large axial discontinuity could have been inherited from the large discontinuities observed in the deep off-axis domains at 48°E using the bathymetry predicted from the satellite data (Fig. 3a). However, the lack of multibeam bathymetry data to the west of 49°E does not allow further analysis. The off-axis traces of the present-day axial discontinuities can be followed up to the outward-facing outer slopes (Fig. 3). The past activity of the magmatically robust segment #27 in the shallow off-axis domains is revealed by large abyssal hills (60 km long, 10–20 km width and 500–900 m high) with a steep faulted scarp facing towards the axis and a gentle dipping outward-facing slope crowned by numerous conical seamounts (Mendel *et al.* 2003). These abyssal hills look like the large abyssal hills (10–16 km wide and 600–700 m high) observed in the ridge section between the Andrew Bain and Prince

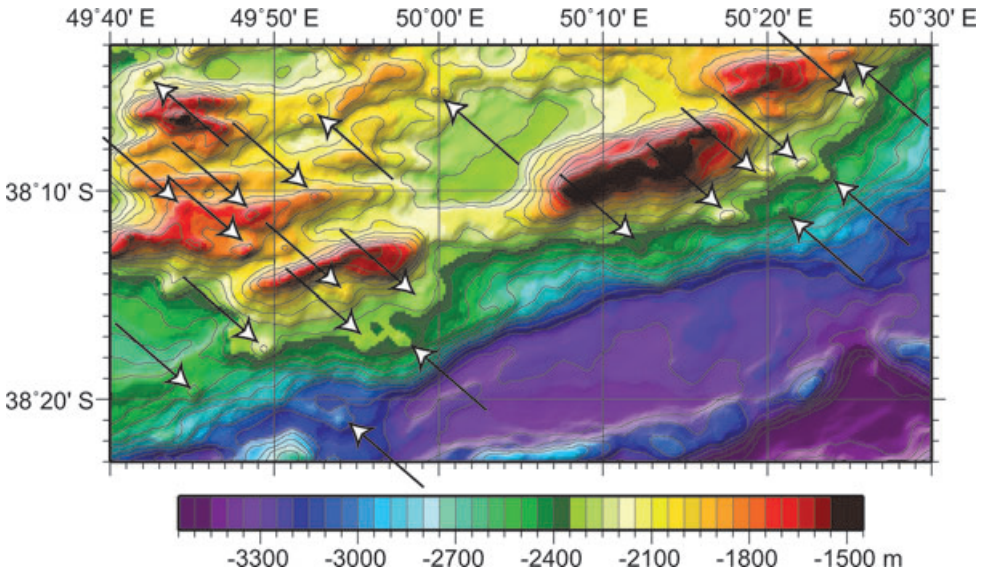

Figure 5. Bathymetric map of the southern outward facing slope bounding the anomalously shallow off-axis domain on the Antarctic Plate. Black and white arrows show rounded shaped features suggesting a volcanic constructional origin. Contour interval is every 100 m.

Edwards TFs near the Marion hotspot (Grindlay *et al.* 1996; Mendel *et al.* 2003). By contrast, they are up to 15 km wider and 500 m higher than the abyssal hills observed in the deeper section of the SWIR between the Gallieni and Melville TFs (Hosford *et al.* 2003; Mendel *et al.* 2003).

The ages determined for the southern branch of the V-shaped shallow off-axis domains in the GALLiENi survey area would correspond to an eastward propagation of the emplacement of the shallow off-axis domains 8.1–4.2 Ma ago, at a mean rate of ∼30 km Ma^{-1} (twice the spreading rate). However, the outer slope of the southern shallow off-axis domain has an en-échelon shape with sections, which are nearly spreading-perpendicular, and at least 3 and possibly four sections which are more oblique (Fig. 3). This indicates that the propagation probably did not occur progressively at this average rate of 30 km Ma^{-1} over the 8.1–4.2 Ma time period, but faster over at least three and possibly four shorter time periods. Two of the more oblique sections of the southern outer slope coincide with the off-axis traces of the east and west ends of segment #27 (at about 50°05'E and 50°50'E; Figs 3a and b). This could indicate that the propagation of the emplacement of the shallow off-axis domains was discontinuous with small jumps of the ridge axis to the northeast inducing the formation of new axial discontinuities and no or little propagation meanwhile during the early construction of the segments.

5 DISCUSSION

5.1 A melt supply anomaly and its along-axis propagation

Seafloor accreted along the SWIR between the Indomed and the Gallieni TFs over the past ∼10 Myr is locally much shallower and corresponds to thicker crust than seafloor accreted previously along the same ridge region. The outward facing topographic gradients marking the outer edges of the off-axis shallow domains are at least partially, volcanic constructions (Fig. 5). Their vertical relief (>2000 m locally) and their geometry, parallel to the present-day axis along a >210-km-long ridge section, suggest an extremely sudden and large event dated between ∼8 and ∼11 Ma (Figs 3 and 6). Asymmetric spreading and small ridge jumps occur at the onset of the formation of the shallow off-axis domains, leading to a reorganization of the ridge segmentation. To the east of ∼49°30'E towards the Gallieni TF, and possibly also to the west of ∼47°15'E towards the Indomed TF (Fig. 3), the age of the outer edges of the shallow off-axis domains decreases indicating along-axis propagation of this event towards these TFs since ∼8 Ma. At present, except at the centre of the magmatically robust segment #27, the axial valley is deeper and characterized by possibly thinner gravity-derived model crust than the shallow off-axis domains. We interpret these shallow off-axis domains as the relicts of a volcanic plateau due to a sudden increase of the magma supply which is still active at segment #27 but which has ended along the remaining part of the studied ridge section. We therefore interpret the present-day axial valley, which appears to propagate into segment #27, as partly the result of the rifting of this volcanic plateau.

The mean depth difference between the shallow off-axis domains and the older and deeper off-axis domains (∼1 km in the GALLiENi survey area), is equivalent to the difference between the mean present-day axial depths of the ridge sections to the east and to the west of the Gallieni TF (Cannat *et al.* 1999b; Fig. 2). Based on modelled relationships between regional axial depth, and mantle temperature and melt supply (Klein & Langmuir 1987; White *et al.* 1992), this difference in mean depth suggests that the melt anomaly responsible for the formation of the shallow off-axis domains in our study area had an amplitude of about ∼2 km, and could have corresponded to melting of a ∼40 °C hotter subaxial mantle [see Cannat *et al.* (2004) for explanations on the 1-D analytical model of mantle melting derived from Langmuir *et al.* (1992) and taking into account the effect of upper-mantle conductive cooling at the top of the melting regime in a similar way to the corner flow 2-D model of Bown & White (1994)]. The reduction in melt supply to the east of the Gallieni TF may also be partly ascribed to a decrease in the rate of mantle upflow due to the highest ridge axis obliquity there (Dick *et al.* 2003). However, the corresponding decrease of effective spreading rate (the half-spreading rate resolved in the ridge-perpendicular direction, Dick *et al.* 2003) is less than 1 km Myr^{-1} (from 6.8 to 6 km Myr^{-1}). Using the analytical model of mantle melting of Cannat *et al.* (2004), we estimate that the effect of ridge obliquity on melt production is significant (resulting in a

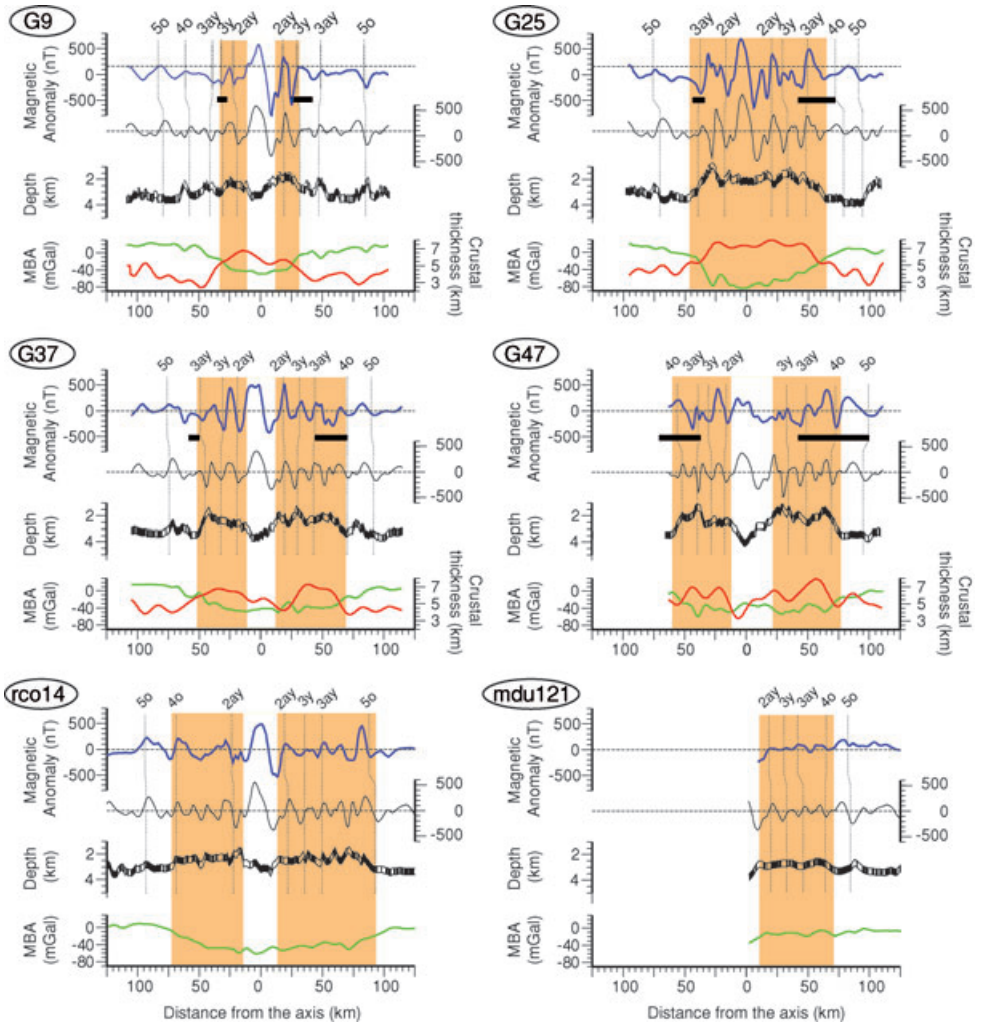

Figure 6. Magnetic anomaly, bathymetric and gravimetic profiles from the RCO1401, SWIFT and GALLiENi cruises across the off-axis shallow domains (in orange) between the Indomed and the Gallieni TFs. MBA profiles are shown in green. Crustal thickness variations (in red) are from Mendel *et al.* (2003). The bathymetric profiles are shown in black. The magnetic anomaly profiles (in blue) are compared with synthetic magnetic anomaly profiles calculated using the geomagnetic reversal timescale of Cande & Kent (1995) and assuming a 15 km Myr^{-1} spreading rate at 49°E/−38°N (Lemaux *et al.* 2002) and a constant 500-m-thick magnetic layer draped on the bathymetry with a 14 A m^{-1} magnetization for the Brunhes period and a uniform ±7 A m^{-1} magnetization off-axis. We modelled the transition zone between two inversely magnetized blocks using the method of Tisseau & Patriat (1981) and Mendel *et al.* (2005). Thick black lines underline sections of the profiles with highly asymmetric spreading rates (>30 per cent). We trace the outer edges of the off-axis shallow domains at the foot of the large outward facing topographic gradients where the vertical relief exceeds ∼2000 m (i.e. in profiles G25, G37 and G47). In areas where the off-axis shallow domains are less well marked in the topography (i.e. in profiles G9, rco14 and mdu121) we also used the lateral continuity of these domains in plan view (e.g. Fig. 3) to identify their edges.

∼300 m crustal thickness decrease) but not enough to explain the observed variations in regional axial depth and Na8.0 content of basalts on each side of the Gallieni TF. Moreover, isochrones in the deep off-axis domains show that the overall ridge geometry between the Indomed and Gallieni TFs is stable for the last 33 Myr (Patriat *et al.* 2008). We therefore conclude that the melt supply anomaly in this ridge region is not produced by a change of the ridge obliquity.

This event of higher melt supply started in the central part of the ridge section between the Indomed and the Gallieni TFs. It then propagated along axis to the east and probably also to the west towards these TFs, but did not cross them. The Gallieni TF coincides with a distinct step in the isotopic compositions of present-day basalts in Pb and to a lesser extent in Nd (Meyzen *et al.* 2005). This suggests that there is presently no continuity in mantle flow beneath this TF (Meyzen *et al.* 2005). The ridge sections near the Bouvet and Marion hotspots also display gravity and bathymetric anomalies that are confined between large fracture zones (Andrew Bain and Discovery II TFs), suggesting that large offset transforms are capable of inhibiting or even blocking along-axis melt flow (Georgen *et al.* 2001). Such a situation could occur if the mantle flow below the ridge is predominantly shallow and controlled by the connectivity of a low-viscosity, subaxial channel. Numerical modelling with such a simplified channel-flow geometry predicts that TFs reduce the along-axis asthenospheric flow (Georgen & Lin 2003). Along-axis flow stagnates farther upstream from the transform as the transform offset increases (Georgen & Lin 2003). The decreasing width of the off-axis shallow domains towards the Indomed and Gallieni TFs would then reflect such a decreasing of the along-axis flow as the TFs are approached. Additional thermal effects such as a thermal erosion of the TFs caused by anomalously hot material may also gradually favour the propagation of the melting anomaly towards the TFs.

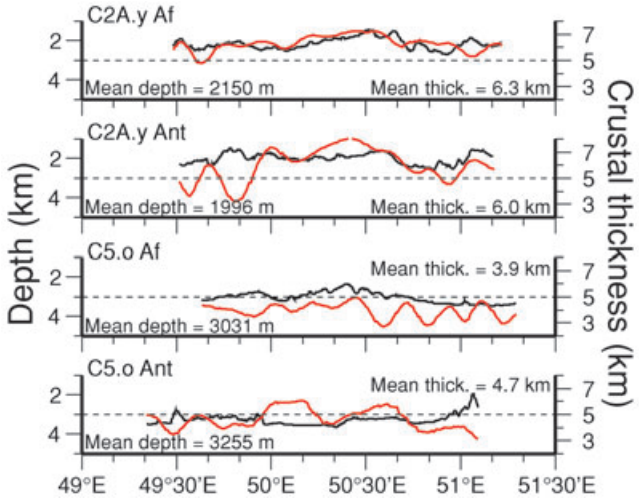

Figure 7. Bathymetric profiles (in black) and crustal thickness variations (in red) from Mendel *et al.* (2003 along the C2A.y and C5.o chrons on both African (Af) and Antarctic (Ant.) plates between 49°15'E and 51°20′E in the GALLiENi cruise survey area.

The along-axis length of the SWIR melting anomaly between the Indomed and Gallieni TFs (580 km) falls in the range of lengths of the V-shaped ridges described near the Azores (∼400 km; Vogt 1976) and near Iceland (∼700 km; Vogt 1976) hotspots. Only one event of enhanced magmatism can be identified on the MAR near the Azores hotspot (Cannat *et al.* 1999a) while the V-shaped ridges south of Iceland occur every 2–6 Myr (Jones *et al.* 2002). Propagating rates of these ridges along the MAR are highly variable [60 and 75–200 km Myr^{-1} near the Azores (Cannat *et al.* 1999a) and Iceland (Vogt 1976; White *et al.* 1995), respectively]. Crustal thickness variations and inferred mantle temperature anomaly on the SWIR are close to those estimated south of Iceland (2 km and 30°C; White *et al.* 1995) while the crust may be more than 5 km thicker and the mantle temperature variation may reach 35 or 70 °C at the Azores [depending on the type of melting model used to estimate the MORB production (Cannat *et al.* 1999a; Asimow *et al.* 2004)].

5.2 Hotter mantle temperatures between the Indomed and Gallieni TFs than in the neighbouring ridge sections: influence of the Crozet hotspot?

Between the Indomed and the Gallieni TFs, both regional axial depth and the along-axis variation of $Na_{8.0}$ content of basalts indicate higher melt production than beneath the neighbouring deeper ridge sections (Cannat *et al.* 2008). The along-axis variations of other geochemical proxies for the extent of partial melting, such as $(Sm/Yb)_n$ or CaO/Al_2O_3, also support higher mantle temperatures in the subaxial mantle of this ridge region (Meyzen *et al.* 2003). A prominent MBA low also suggests thicker crust and/or a hotter mantle beneath this shallow region of the present-day SWIR (Fig. 2).

We extracted lateral variations in shear velocity from the surface wave tomography of fundamental and higher mode Rayleigh waves of Debayle *et al.* (2005) to provide new insights into the thermal structure of the upper mantle beneath the SWIR (Fig. 8b). Because *S*-wave velocities are particularly sensitive to temperature, *S*-wave speed maps are valuable for understanding thermal variations in the mantle. Sampling the tomographic model of Debayle *et al.* (2005)

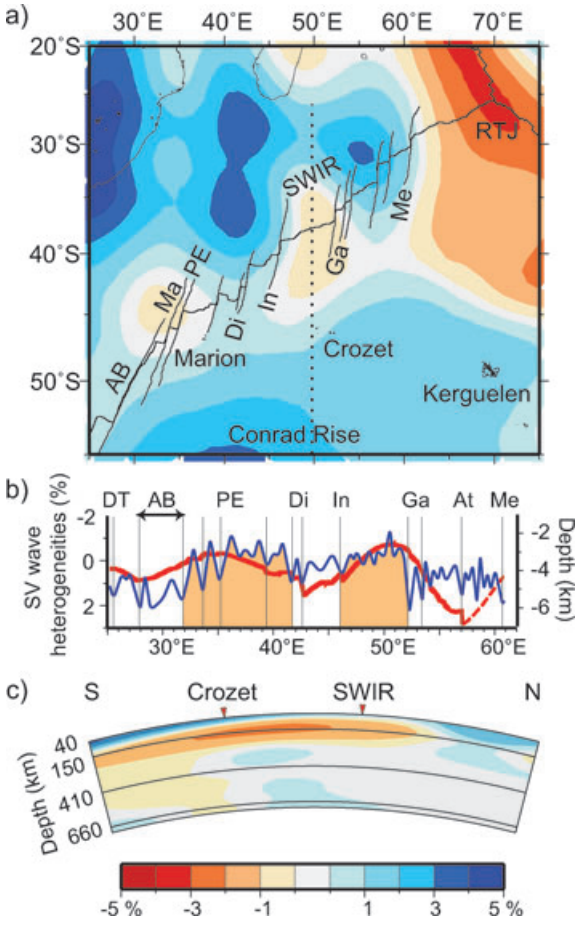

Figure 8. SV-wave heterogeneities under the SWIR domain from the tomographic model of Debayle *et al.* (2005). (a) Map of the SV-wave heterogeneities at 75 km depth. SV-wave perturbations are in per cent relative to PREM (reference $Vs = 4.39$ km s^{-1} at 75 km depth Dziewonski & Anderson 1981). The NS dotted line at 50°E indicates the location of the cross section shown in (c). (b) Comparison between the smoothed along-axis depth profile (blue line) along the axis of the SWIR between the Du Toit and the Melville TFs and the along-axis variation of the SV-wave heterogeneity at 75 km depth (red line). To the east of the Atlantis II TF the *S*-waves velocity decrease (dashed red line) is due to the lack of resolution of the tomographic images and to the influence of the nearby Central and Southeast Indian ridges. The orange areas indicate the two ridge sections with prominent MBA lows and shallow bathymetry as in Figs 1 and 2. (c) NS striking cross-section at 50°E in the tomographic model. DT, AB, Ma, PE, ES, Di, In, Ga, At and Me as in Fig. 1.

along the SWIR axis at 75 km depth bring out two large negative anomalies of *S*-wave velocities which are centred near 35°E, close to the Prince Edward TF, and near 50°30'E in segment #27 (Fig. 8b). The amplitude of these *S*-wave velocities variations is >2 per cent at 75 km depth (SV-wave perturbations are in per cent relative to PREM velocity reference $Vs = 4.39$ km s^{-1} at 75 km depth; Dziewonski & Anderson 1981). We interpret the local fast perturbation in the deeper ridge subsection between the Discovery and Indomed TFs as being a colder region which separates the two large negative *S*-waves anomalies reflecting hotter mantle areas (Fig. 8). Shear wave velocities are strongly increasing along the Andrew Bain TF system and in the oblique ridge subsection east of the Gallieni TF. The tomographic model of Debayle *et al.* (2005) at 75 km depth also show a significant slow seismic anomaly beneath the SWIR elongated in the north–south direction and centred close

to the ridge axis, between the Indomed and Gallieni TFs (Fig. 8a). This shallow anomaly is connected at depth to a large low velocity anomaly present at the bottom of the oceanic lithosphere. This large anomaly is elongated in the NE–SW direction, with a lateral extension greater than 1000 km. It has a maximum slow velocity perturbation near 150 km depth, between the SWIR and the Conrad Rise (Fig. 8c). Previous studies (Debayle & Sambridge 2004) have shown that such structures are well resolved in Debayle *et al.* (2005) model. The shallow slow anomaly at 75 km depth (Fig. 8a) is much weaker (∼1 per cent slower than PREM) than the anomalies detected along the MAR close to the Azores and Iceland hotspots (∼ −3.5 to −4 per cent; Pilidou *et al.* 2005) which would suggest a weaker thermal anomaly beneath the SWIR than beneath the MAR. It also decays to the PREM background level below ∼200 km depth beneath the Crozet bank (Fig. 8). No low-velocity anomalies were found that might be interpreted as plume stems beneath this hotspot. However, this does not rule out the existence of plume stems, as such narrow features (∼200 km) are not expected to be properly resolved in the deep part of the model (Debayle *et al.* 2005). We therefore suggest that the hot (low-velocity) anomaly beneath the SWIR between the Indomed and the Gallieni TFs is produced by the Crozet hotspot. Higher mantle temperatures in this region would have led to an event of enhanced magmatism ∼10 Ma ago and to the construction of a large volcanic plateau.

A recent investigation of helium and trace elements variations along the SWIR reveals that the SWIR section located between the Indomed and Gallieni TFs displays a large primitive helium anomaly ($^4He/^3He < 80\,000$; Gautheron *et al.* 2008, submitted). Such primitive helium isotopic ratios are distinctively lower than the homogeneous helium isotopic ratio in MORBs ($^4He/^3He \sim 90\,000$), indicating a contribution of an undegassed and undepleted OIB source (Allegre *et al.* 1983). However, along the Indomed–Gallieni section, while He isotopic systematics indicate the presence of a primitive component, other geochemical proxies for the level of mantle depletion or enrichment in incompatible elements (such as K_2O/TiO_2 and La/Sm) rather show the presence of a depleted mantle source (Gautheron *et al.* 2008, submitted). Although there is no consensus regarding the trace element and Sr-Nd-Pb-Hf isotopic signature of the low $^4He/^3He$ component sampled by many OIBs and MORBs around the world (Kurz *et al.* 1998, 2005; Jackson *et al.* 2007), it is clear that this component includes significant portions of depleted mantle material (Kurz *et al.* 1998; Stuart *et al.* 2003; Ellam & Stuart 2004; Gautheron *et al.* submitted; Starkey *et al.* 2009). The geochemical signature of basalts from the Indomed–Gallieni ridge section could be, therefore, consistent with a contribution of material arising from the Crozet hotspot. However, the few helium isotopic data for this hotspot display MORB-like isotopic ratios (∼90 000; Gautheron *et al.*, submitted). Without additional sampling and geochemical data for the Crozet hotspot, it is therefore presently difficult to speculate further on its potential geochemical influence along the SWIR. Alternatively, the recent observation that U and Th may be less compatible than He during mantle melting (Parman *et al.* 2005; Heber *et al.* 2007) has also led to the suggestion that ancient melt depletion event during the earth history can freeze the $^4He/^3He$ ratio to low values (Graham *et al.* 1990; Class & Goldstein 2005; Parman *et al.* 2005). Such an ancient melt depletion event could explain at first order the multi-elemental geochemical signature of basalts from the Indomed–Gallieni ridge section, but the former domains of depleted mantle would then be highly refractory and would tend to starve the melt supply to the ridge which is inconsistent with the high melt production estimated for this ridge section. We therefore favour the hypothesis of a deep, hot and primitive-He-rich source, which might be related to the Crozet hotspot. We thus suggest that the Crozet hotspot could trigger small upper-mantle thermal plumes rising beneath the SWIR and incorporating small amounts of lower mantle material during plume formation. These mantle thermal plumes could produce focused events of enhanced magmatism such as the one observed in this study.

The long ridge-hotspot distance of more than 1000 km from the Crozet bank to the SWIR may be put forward to argue that the Crozet hotspot is unlikely to interact with the SWIR. Theoretical relations and observations at other hotspots show a decrease of the along-axis plume length with increasing plume–ridge separation until becoming insignificant at distances more than about 500 km (Ito & Lin 1995; Ribe *et al.* 1995; Ito *et al.* 2003). However, there are a number of exceptions to this tendency. Geochemical data suggest, for example, that the Kerguelen and La Réunion hotspots may still exert residual influence on the southeast and on the central Indian ridges, respectively, although located more than 1000 km from these ridges (Mahoney *et al.* 1989; Graham *et al.* 1999). Off-axis volcanic chains or lineaments (e.g. Rodrigues ridge) occur between these ridges and the hotspot centres (Small 1995; Dyment *et al.* 2007). Measurements of 23 separate oceanic hotspots (excluding the Crozet hotspot) show a nearly linear increase in volcanic lineament length with increasing age of the plate at the hotspot and increasing plume–ridge separation distance (Mittelstaedt & Ito 2005). This linear relationship holds until plate ages of ∼25 Ma and plume–ridge separation distances in excess of ∼1250 km (Mittelstaedt & Ito 2005). This is in agreement with the absence of lineament between the Crozet hotspot (sitting on a late cretaceous lithosphere) and the SWIR (Fig. 1). Beyond 25 Ma, plate thicknesses may be too large for plume stresses to enhance the ability of magma to penetrate the plate (Mittelstaedt & Ito 2005).

CONCLUDING REMARKS

The SWIR section between the Indomed and Gallieni TFs displays physical characteristics, which may be consistent with the interaction with a hotspot. We have documented an event of enhanced magmatism starting ∼10 Ma ago which may be ascribed to a regionally higher mantle temperature provided by mantle outpouring from the Crozet hotspot towards the SWIR. Clearly, further sampling of the flanks of the SWIR and imaging of the oceanic crust and mantle are needed to assess the hypothesis of an SWIR–Crozet interaction and particularly to provide new constraints on the mantle reservoir and the volume, distribution and composition of melts beneath this ridge section.

ACKNOWLEDGMENTS

We thank officers and crew of the R/V Marion Dufresne for their assistance during the 'SWIFT' cruise. We also thank two anonymous reviewers for very constructive reviews and suggestions. Figures were created using the public domain GMT software (Wessel & Smith 1995). Participation to the cruise and post-cruise studies were supported by the Centre National de la Recherche Scientifique (CNRS-INSU).

REFERENCES

Allegre, C.J., Staudacher, T., Sarda, P. & Kurz, M., 1983. Constraints on evolution of Earth's mantle from rare gas systematics, *Nature,* **303,** 762–766.

Asimow, P.D., Dixon, J.E. & Langmuir, C.H., 2004. A hydrous melting and fractionation model for mid-ocean ridge basalts: application to the Mid-Atlantic Ridge near the Azores, *Geochem. Geophys. Geosyst.,* **5,** Q01E16, doi:10.1029/2003GC000568.

Bird, P., 2003. An updated digital model of plate boundaries, *Geochem. Geophys. Geosyst.,* **4,** doi:10.1029/2001GC000252.

Bown, J.W. & White, R.S., 1994. Variation with spreading rate of oceanic crustal thickness and geochemistry, *Earth planet. Sci. Lett.,* **121,** 435–449.

Cande, S.C. & Kent, D.V., 1995. Revised calibration of the geomagnetic polarity timescale for the Late Cretaceous and Cenozoic, *J. geophys. Res.,* **100,** 6093–6095.

Cannat, M. *et al,*. 1999a. Mid-Atlantic ridge-Azores hotspot interactions: along-axis migration of a hotspot-derived magmatic pulse 14 to 4 Myrs ago, *Earth planet. Sci. Lett.,* **173,** 257–269.

Cannat, M., Rommevaux-Jestin, C., Sauter, D., Deplus, C. & Mendel, V., 1999b. Formation of the axial relief at the very slow spreading Southwest Indian Ridge (49°-69°E), *J. geophys. Res.,* **104,** 22 825–22 843.

Cannat, M., Cann, J. & Maclennan, J., 2004. Some hard rock constraints on the supply of heat to mid-ocean ridges. in *The Thermal Structure of the Ocean Crust and Dynamics of Hydrothermal Circulation,* pp. 111–149, eds German, C., Lin, J. & Parson, L., American Geophysical Union, Washington, DC.

Cannat, M., Sauter, D., Bezos, A., Meyzen, C., Humler, E. & Le Rigoleur, M., 2008. Spreading rate, spreading obliquity, and melt supply at the ultraslow spreading Southwest Indian Ridge, *Geochem. Geophys. Geosyst.,* **9,** Q04002.

Charvis, P., Recq, M., Operto, S. & Brefort, D., 1995. Deep structure of the northern Kerguelen Plateau and hotspot-derived activity, *Geophys. J. Int.,* **122,** 899–924.

Chevallier, L. & Nougier, J., 1981. Première étude volcano-structurale de l'Ile de la Possession, îles Crozet (TAAF), Océan Indien Austral, *Comptes Rendus de l' Académie des Sciences Série IIa:Sciences de la Terre et des Planètes,* **292,** 363–368.

Chu, D. & Gordon, R.G., 1999. Evidence for motion between Nubia and Somalia along the Southwest Indian Ridge, *Nature,* **398,** 64–67.

Class, C. & Goldstein, S.L., 2005. Evolution of helium isotopes in the Earth's mantle, *Nature,* **436,** 1107–1112.

Courtney, R.C. & Recq, M., 1986. Anomalous heat flow near the Crozet plateau and mantle convection, *Earth planet. Sci. Lett.,* **79,** 373–384.

Curray, J.R. & Munasinghe, T., 1991. Origin of the Rajmahal traps and the 85°E ridge: preliminary reconstructions of the trace of the Crozet hotspot, *Geology,* **19,** 1237–1240.

Debayle, E. & Sambridge, M., 2004. Inversion of massive surface wave data sets: model construction and resolution assessment, *J. geophys. Res.,* **109**(B02316), doi:10.1029/2003JB002652.

Debayle, E., Kennett, B. & Priestley, K., 2005. Global azimuthal seismic anisotropy and the unique plate-motion deformation of Australia, *Nature,* **433,** 509–512.

Dick, H.J.B., Lin, J. & Schouten, H., 2003. An ultraslow-spreading class of ocean ridge, *Nature,* **426,** 405–412.

Doucelande, R., 2000. Mesure des compositions isotopiques de plomb par spectrométrie de masse à thermo-ionisation: méthode du double spike; Géochimie des panaches mantelliques: approches globale et locale, *PhD thesis*. Institut de Physique du Globe de Paris, Paris.

Duncan, R.A., 1981. Hotspots in the southern oceans-an absolute frame of reference for motion of the Gondwana continents, *Tectonophys.,* **74,** 29–42.

Dupré, B. & Allègre, C., 1983. Pb-Sr isotope variation in Indian Ocean basalts and mixing phenomena, *Nature,* **303,** 142–146.

Dyment, J., Lin, J. & Baker, E.T., 2007. Ridge-HotSpot interactions; what mid-ocean ridges tell us about deep earth processes, *Oceanography,* **20,** 102–115.

Dziewonski, A.M. & Anderson, D.L., 1981. Preliminary reference earth model, *Phys. Earth planet. Inter.,* **25,** 297–356.

Ellam, R.M. & Stuart, F.M., 2004. Coherent He-Nd-Sr isotope trends in high 3He/4He basalts: implications for a common reservoir, mantle heterogeneity and convection, *Earth planet. Sci. Lett.,* **228,** 511–523.

Fisher, R.L. & Goodwillie, A.M., 1997. The physiography of the Southwest Indian Ridge, *Mar. geophys. Res.,* **19,** 451–455.

Gautheron, C., Bezos, A., Moreira, M. & Humler, E., 2008. Helium and trace element geochemical signals in the southwest Indian Ocean, in *Proceedings of the 18th Annual V.M. Goldschmidt Conference,* Geochimica et Cosmochimica Acta, Vancouver, Canada.

Gautheron, C., Bezos, A., Moreira, M. & Humler, E., submitted. Helium and trace element geochemical signals in the southwest indian ocean, *Earth planet. Sci. Lett.,* submitted.

Georgen, J. & Lin, J., 2003. Plume-transform interations at ultra-slow spreading ridges: implications for the Southwest Indian Ridge, *Geochem. Geophys. Geosyst.,* **4**(9), 9106, doi:1010.1029/2003GC000542.

Georgen, J.E., Lin, J. & Dick, H.J.B., 2001. Evidence from gravity anomalies for interactions of the Marion and Bouvet hotspots with the Southwest Indian Ridge: effects of transform offsets, *Earth planet. Sci. Lett.,* **187,** 283–300.

Giret, A., Tourpin, S., Marc, S., Verdier, O. & Cottin, J.-Y., 2002. Volcanisme de l'île aux Pingouins, archipel Crozet, témoin de l'hétérogénéité du manteau fertile au sud de l'océan Indien, *Comptes Rendus Geosciences,* **334,** 481–488.

Goslin, J. & Diament, M., 1987. Mechanical and thermal isostatic response of the Del Cano Rise and Crozet Bank (southern Indian Ocean) from altimetry data, *Earth planet. Sci. Lett.,* **84,** 285–294.

Goslin, J. & Patriat, P., 1984. Absolute and relative plate motions and hypotheses on the origin of five aseismic ridges in the Indian Ocean, *Tectonophys.,* **101,** 221–244.

Graham, D., Lupton, J., Albarede, F. & Condomines, M., 1990. Extreme temporal homogeneity of helium isotopes at Piton de la Fournaise, Reunion Island, *Nature,* **347,** 545–548.

Graham, D.W., Johnston, K.T.M., Priebe, L.D. & Lupton, J.E., 1999. Hotspot-ridge interaction along the Southeast Indian Ridge near Amsterdam and St. Paul islands: helium isotope evidence, *Earth planet. Sci. Lett.,* **167,** 297–310.

Grindlay, N.R., Madsen, J., Rommevaux, C., Sclater, J. & Murphy, S., 1996. Southwest Indian Ridge 15°E-35°E: a geophysical investigation of an ultra-slow spreading mid-ocean ridge system, *InterRidge News,* **5,** 7–12.

Grindlay, N.R., Madsen, J.A., Rommevaux, C. & Sclater, J., 1998. A different pattern of ridge segmentation and mantle Bouguer gravity anomalies alond the ultra-slow spreading Southwest Indian Ridge (15°30'E to 25°E), *Earth planet. Sci. Lett.,* **161,** 243–253.

Hanan, B.B. & Graham, D.W., 1997. Lead and helium isotope evidence from oceanic basalts for a common deep source of mantle plume, *Science,* **272,** 991–995.

Heber, V.S., Brooker, R.A., Kelley, S.P. & Wood, B.J., 2007. Crystal-melt partitioning of noble gases (helium, neon, argon, krypton, and xenon) for olivine and clinopyroxene, *Geochim. Cosmochim. Acta,* **71,** 1041–1061.

Hedge, C.E., Watkins, N.D., Hildreth, R.A. & Doering, W.P., 1973. $^{87}Sr/^{86}Sr$ ratios in basalts from islands in the indian ocean, *Earth planet. Sci. Lett.,* **21,** 29–34.

Horner-Johnson, B.C., Gordon, R.G., Cowles, S.M. & Argus, D.F., 2005. The angular velocity of Nubia relative to Somalia and the location of the Nubia–Somalia–Antarctica triple junction, *Geophys. J. Int.,* **162,** 221–238.

Hosford, A., Tivey, M., Matsumoto, T., Dick, H., Schouten, H. & Kinoshita, H., 2003. Crustal magnetization and accretion at the Southwest Indian Ridge near the Atlantis II fracture zone, 0–25 Ma, *J. geophys. Res.,* **108**(B3), 2169, doi:10.1029/2001JB000604.

Ito, G. & Lin, J., 1995. Oceanic spreading center-hotspot interactions: constraints from along-isochron bathymetry and gravity anomalies, *Geology,* **23,** 657–660.

Ito, G., Lin, J. & Graham, D.W., 2003. Observational and theoretical studies of the dynamics of mantle plume-mid-ocean ridge interaction, *Rev. Geophys.,* **41**(4), 1017, doi:10.1029/2002RG000117.

Jackson, M.G., Kurz, M.D., Hart, S.R. & Workman, R.K., 2007. New Samoan lavas from Ofu Island reveal a hemispherically heterogeneous high 3He/4He mantle, *Earth planet. Sci. Lett.,* **264,** 360–374.

Jones, S.M., White, N. & Maclennan, J., 2002. V-shaped ridges around Iceland: implications for spatial and temporal patterns of mantle convection, *Geochem. Geophys. Geosyst.,* **3**(10), 1059, doi:10.1029/2002GC000361.

Klein, E.M. & Langmuir, C.H., 1987. Global correlations of ocean ridge basalt chemistry with axial depth and crustal chemistry, *J. geophys. Res.,* **92,** 8089–8115.

Kurz, M.D., 1982. Helium isotope geochemistry of oceanic volcanic rocks: implications for mantle heterogeneity and degassin, *Doctor of Philosophy,* Massachusetts Institute of Technology and Woods Hole Oceanographic Institution.

Kurz, M.D., le Roex, A.P. & Dick, H.J.B., 1998. Isotope geochemistry of the oceanic mantle near the Bouvet triple junction, *Geochim. Cosmochim. Acta,* **62,** 841–852.

Kurz, M.D., Moreira, M., Curtice, J., Lott, D.E. III, Mahoney, J.J. & Sinton, J.M., 2005. Correlated helium, neon, and melt production on the superfast spreading East Pacific Rise near 17°S, *Earth planet. Sci. Lett.,* **232,** 125–142.

Langmuir, C.H., Klein, E.M. & Plank, T., 1992. Petrological systematics of mid-ocean ridge basalts: constraints on melt generation beneath mid-ocean ridges. in *Mantle Flow and Melt Generation at Mid-Ocean Ridges,* pp. 183–280, eds Phipps Morgan, J., Blackman, D.K. & Sinton, J.M., American Geophysical Union, Washington, DC.

Lemaux, J., Gordon, R.G. & Royer, J.Y., 2002. Location of the Nubia-Somalia boundary along the Southwest Indian Ridge, *Geology,* **30,** 339–342.

Mahoney, J., Nicollet, C. & Dupuy, C., 1991. Madagascar basalts: tracking oceanic and continental sources, *Earth planet. Sci. Lett.,* **104,** 350–363.

Mahoney, J., LeRoex, A.P., Peng, Z., Fisher, R.L. & Natland, J.H., 1992. Southwestern limits of Indian ocean ridge mantle and origin of low 206 Pb/204 Pb mid-ocean ridge basalt: isotope systematics of the Central Southwest Indian Ridge (17-50°E), *J. geophys. Res.,* **97,** 19 771–19 790.

Mahoney, J.J., Natland, J.H., White, W.M., Poreda, R., Bloomer, S.H., Fisher, R.L. & Baxter, A.N., 1989. Isotopic and geochemical provinces of the western indian ocean spreading centers, *J. geophys. Res.,* **94,** 4033–4052.

Mahoney, J.J., White, W.M., Upton, B.G.J., Neal, C.R. & Scrutton, R.A., 1996. Beyond EM-1: lavas from Afanasy-Nikitin Rise and the Crozet Archipelago, Indian Ocean, *Geology,* **24,** 615–618.

Mendel, V., Sauter, D., Rommevaux-Jestin, C., Patriat, P., Lefebvre, F. & Parson, L.M., 2003. Magmato-tectonic cyclicity at the ultra-slow spreading Southwest Indian Ridge: evidence from variations of axial volcanic ridge morphology and abyssal hills pattern, *Geochem. Geophys. Geosyst.,* **4**(5), 9102, doi:10.1029/2002GC000417.

Mendel, V., Munschy, M. & Sauter, D., 2005. MODMAG, a MATLAB program to model marine magnetic anomalies, *Comput. Geosci.,* **31,** 589–597.

Meyzen, C., 2002. Pétrogenèse des MORB dans les zones froides du manteau supérieur Indien: La ride sud-ouest indienne et la discordance australo-antarctique, *PhD thesis*. Institut National Polytechnique de Lorraine, Nancy, France.

Meyzen, C.M., Toplis, M.J., Humler, E., Ludden, J.N. & Mével, C., 2003. A discontinuity in mantle composition beneath the southwest Indian Ridge, *Nature,* **421,** 731–733.

Meyzen, C.M., Ludden, J.N., Humler, E., Luais, B., Toplis, M.J., Mével, C. & Storey, M., 2005. New insights into the origin and distribution of the DUPAL isotope anomaly in the Indian Ocean mantle from MORB of the Southwest Indian Ridge, *Geochem. Geophys. Geosyst.,* **6**(11), Q11K11, doi:10.1029/2005GC000979.

Meyzen, C.M., Blichert-Toft, J., Ludden, J.N., Humler, E., Mével, C. & Albarède, F., 2007. Isotopic portrayal of the Earth's upper mantle flow field, *Nature,* **447,** 1069–1074.

Mittelstaedt, E. & Ito, G., 2005. Plume-ridge interaction, lithospheric stress, and the origin of near-ridge volcanic lineations, *Geochem. Geophys. Geosyst.,* **6,** Q06002, doi:10.1029/2004GC000860.

Monnereau, M. & Cazenave, A., 1990. Depth and geoid anomalies over oceanic hotspot swells: a global survey, *J. geophys. Res.,* **95,** 15 429–15 438.

Montelli, R., Nolet, G., Dahlen, F.A., Masters, G. & Hung, S.-H., 2004. Finite-frequency tomography reveals a variety of plumes in the mantle, *Science,* **303,** 338–343.

Morgan, W.J., 1981. Hotspot tracks and the opening of the Atlantic and Indian oceans, in *The Oceanic Lithosphere,* pp. 443–487, ed. Emiliani, C., Wiley Interscience, New York.

Müller, R.D., Royer, J.Y. & Lawver, L.A., 1993. Revised plate motions relative to the hotspots from combined Atlantic and Indian Ocean hotspot tracks, *Geology,* **21,** 275–278.

Munschy, M. & Schlich, R., 1990. Etude géophysique des dorsales de l'océan Indien dans la région du point triple de Rodriguez, *Oceanol. Acta,* **10,** 119–128.

O'Neill, C., Müller, D. & Steinberger, B., 2003. Geodynamic implications of moving Indian Ocean hotspots, *Earth planet. Sci. Lett.,* **215,** 151–168.

Parman, S.W., Kurz, M.D., Hart, S.R. & Grove, T.L., 2005. Helium solubility in olivine and implications for high 3He/4He in ocean island basalts, *Nature,* **437,** 1140–1143.

Parsons, B. & Sclater, J.G., 1977. An analysis of the variation of ocean floor bathymetry and heat flow with age, *J. geophys. Res.,* **82,** 803–827.

Patriat, P., Sauter, D., Munschy, M. & Parson, L.M., 1997. A survey of the Southwest Indian Ridge axis between Atlantis II Fracture Zone and the Indian Triple Junction: regional setting and large scale segmentation, *Mar. geophys. Res.,* **19,** 457–480.

Patriat, P., Sloan, H. & Sauter, D., 2008. From slow to ultra-slow: a previously undetected event at the Southwest Indian Ridge at ∼24Ma, *Geology,* **36,** 207–210.

Pilidou, S., Priestley, K., Debayle, E. & Gudmundsson, Ó., 2005. Rayleigh wave tomography in the North Atlantic: high resolution images of the Iceland, Azores and Eifel mantle plumes, *Lithos,* **79,** 453–474.

Recq, M., Goslin, J., Charvis, P. & Operto, S., 1998. Small-scale crustal variability within an intraplate structure: the Crozet Bank (southern Indian ocean), *Geophys. J. Int.,* **134,** 145–156.

Ribe, N., Christensen, U.R. & Theißing, J., 1995. The dynamics of plume-ridge interaction, 1: ridge-centered plumes, *Earth planet. Sci. Lett.,* **134,** 155–168.

Rommevaux-Jestin, C., Deplus, C. & Patriat, P., 1997. Mantle Bouguer anomaly along a super-slow spreading ridge: comparison with central Mid-Atlantic ridge and implications on the accretionary process, *Mar. geophys. Res.,* **19,** 481–503.

Salters, V.J.M. & White, W.M., 1998. Hf isotope constraints on mantle evolution, *Chem. Geol.,* **145,** 447–460.

Sandwell, D.T. & Smith, W.H.F., 1997. Marine gravity anomaly from Geosat and ERS-1 satellite altimetry, *J. geophys. Res.,* **102,** 10 039–10 054.

Sauter, D., Patriat, P., Rommevaux-Jestin, C., Cannat, M., Briais, A. & the Gallieni Shipboard and Scientific Party, 2001. The Southwest Indian Ridge between 49°15'E and 57°E: focused accretion and magma redistribution, *Earth planet. Sci. Lett.,* **192,** 303–317.

Sauter, D., Carton, H., Mendel, V., Munschy, M., Rommevaux-Jestin, C., Schott, J.-J. & Whitechurch, H., 2004. Ridge segmentation and the magnetic structure of the Southwest Indian Ridge (at 55°30'E, 55°30'E and 66°20′E): implications for magmatic processes at ultraslow-spreading centers, *Geochem. Geophys. Geosyst.,* **5,** Q05K08, doi:10.1029/2003GC000581.

Searle, R.C., Keeton, J.A., Owens, R.B., White, R.S., Mecklenburgh, R., Parsons, B. & Lee, S.M., 1998. The Reykjanes Ridge: structure and tectonics of a hot-spot-influenced, slow-spreading ridge, from multibeam bathymetry, gravity and magnetic investigations, *Earth planet. Sci. Lett.,* **160,** 463–478.

Seyler, M., Cannat, M. & Mével, C., 2003. Evidence for major-element heterogeneity in the mantle source of abyssal peridotites from the Southwest Indian Ridge (52° to 69°E), *Geochem. Geophys. Geosyst.,* **4**(2), 9101, doi:1029/2002GC000305.

Small, C., 1995. Observations of ridge-hotspot interactions in the Southern Ocean, *J. geophys. Res.,* **100,** 17 931–17 946.

Smith, W.H. & Sandwell, D.T., 1997. Global seafloor topography from satellite altimetry and ship depth soundings, *Science,* **227,** 1956–1962.

Starkey, N.A., Stuart, F.M., Ellam, R.M., Fitton, J.G., Basu, S. & Larsen, L.M., 2009. Helium isotopes in early Iceland plume picrites: constraints on the composition of high 3He/4He mantle, *Earth planet. Sci. Lett.,* **277,** 91–100.

Storey, M., Mahoney, J.J., Sauders, A.D., Duncan, R.A., Kelley, S.P. & Coffin, M.F., 1995. Timing hot spot-related volcanism and the breakup of Madagascar and India, *Science,* **267,** 852–855.

Stuart, F.M., Lass-Evans, S., Godfrey Fitton, J. & Ellam, R.M., 2003. High 3He/4He ratios in picritic basalts from Baffin Island and the role of a mixed reservoir in mantle plumes, *Nature,* **424,** 57–59.

Tao, C. *et al.,* 2007. Discovery of the first active hydrothermal vent field at the ultraslow spreading Southwest Indian Ridge: the Chinese DY115–19 Cruise, *InterRidge News,* **16,** 25–26.

Tisseau, J. & Patriat, P., 1981. Identification des anomalies magnétiques sur les dorsales à faible taux d'expansion: Méthode des taux fictifs, *Earth planet. Sci. Lett.,* **52,** 381–396.

Vogt, P.R., 1976. Plumes, subaxial pipe flow, and topography along the mid-oceanic ridge, *Earth planet. Sci. Lett.,* **29,** 309–325.

Wessel, P. & Smith, W.H.F., 1995. New version of Generic Mapping Tools released, *EOS, Trans. AGU,* **76,** 329.

White, R.S., McKenzie, D. & O'Nions, K., 1992. Oceanic crustal thickness from seismic measurements and rare earth element inversions, *J. geophys. Res.,* **97,** 19 683–19 715.

White, R.S., Bown, J.W. & Smallwood, J.R., 1995. The temperature of the Iceland plume and origin of outward-propagating V-shaped ridges, *J. Geol. Soc. Lond.,* **152,** 1039–1045.

Wolfe, C.J., Bjarnason, I.T., VanDecar, J.C. & Solomon, S.C., 1997. Seismic structure of the Iceland mantle plume, *Nature,* **385,** 245–247.